

Predicting Glass-to-Glass and Liquid-to-Liquid Phase Transitions in Supercooled Water using Classical Nucleation Theory

Robert F. Tournier^{1,2}

¹*Univ. Grenoble Alpes, Inst. NEEL, F-38042 Grenoble Cedex 9, France*

²*CNRS, Inst. NEEL, F-38042 Grenoble, France*

E-mail address: robert.tournier@neel.cnrs.fr

Abstract:

Glass-to-glass and liquid-to-liquid phase transitions are observed in bulk and confined water, with or without applied pressure. They result from the competition of two liquid phases separated by an enthalpy difference depending on temperature. The classical nucleation equation of these phases is completed by this quantity existing at all temperatures, a pressure contribution, and an enthalpy excess. This equation leads to two homogeneous nucleation temperatures in each liquid phase; the first one (T_{n-} below T_m) being the formation temperature of an “ordered” liquid phase and the second one corresponding to the overheating temperature (T_{n+} above T_m). Thermodynamic properties, double glass transition temperatures, sharp enthalpy and volume changes are predicted in agreement with experimental results. The first-order transition line at $T_{LL}=0.833\times T_m$ between fragile and strong liquids joins two critical points. Glass phase above T_g becomes “ordered” liquid phase disappearing at T_{LL} at low pressure and at $T_{n+}=1.302\times T_m$ at high pressure.

1- Introduction:

Multiple liquid-to-liquid phase transitions (LLPTs) that are observed in several metallic glass-forming melts, have already been predicted using a classical nucleation equation completed by an enthalpy difference of two liquid phases depending on the square of the reduced temperature $\theta=(T-T_m)/T_m$, where T_m is the melting temperature [1]. The objectives of this paper are to extend the application of this renewed equation to the thermodynamic properties of water, to explain the occurrence of glass-to-glass phase transitions in amorphous water, and to show that the low-density phases obtained under decompression are glass phases analogous to those produced by vapour deposition at temperatures close to T_g [2-5].

First-order transformations under pressure, induce high density amorphous phase [6-14], because the pressure increases the enthalpy and facilitates the glass transformation towards an equilibrium phase of higher density. These enthalpy and entropy changes cannot exceed in principle the value of the frozen enthalpy and entropy [15]. Any glass freezes enthalpy and entropy below T_g , which are available for exothermic relaxation or first-order transitions.

The water glass state is obtained by vapor deposition, liquid hyperquenching, confined water cooling, and application of high pressure to ice followed by various relaxation annealing [16]. A warming

of bulk, amorphous water produces an endothermic event just below the crystallization temperature, occurring at around 136 K. [17-19]. The glass transition is characterized by a specific heat jump preceding the occurrence of crystallization. Applying high pressure to ice, reduces T_m and produces amorphous water. Sharp transformations, viewed as first-order transitions are observed under pressure at 77 K, as well as at higher temperatures. These findings show that a bulk, amorphous liquid that has a low density can be transformed under pressure into a high-density amorphous liquid [6,9,18]. Three amorphous states have been identified under pressure: low density amorphous (LDA); high density amorphous I (HDA); and very high density amorphous (VHDA) after quenching to 77 K. Transformations of LDA to HDA and VHDA are observed after pressure is increased up to 16 kbar, and decompression taken down to residual pressures at temperatures lower than T_g . Some VHDA, HDA and LDA have been studied after complete decompression, down to temperatures of 77 K [7,10,20]. HDA obtained after decompression down to 100 bar and at a temperature of 77 K is also transformed by heating at ~ 140 K in LDA [7]. HDA is recovered by a new compression at $p=0.32$ GPa.

Measurements of water confined within silica gel in 1.1nm pores show the existence of a broad and high specific heat peak, at 227.5 K. (-45.6°C), and two heat flow changes at 124–136 K and 163–173 K, indicating the presence of two glass transitions [21,22]. A pronounced minimum of compressibility is still observed in water at a temperature of $+45.5^\circ\text{C}$, which is symmetrical with regard to T_m at the ambient pressure of the transition at -45.6°C [23,24]. A sharp specific heat increase below 273 K (already equal to $30 \text{ J.K.}^{-1}\text{mole}^{-1}$ at 235 K) is still observed in bulk supercooled water at ambient pressure, down to the crystallization temperature [16,25]. This confirms the possible existence, in the absence of crystallization, of a LLTP at temperatures smaller than 235 K [21,26].

In the first model (of two liquids), these phenomena are attributed, to the existence of a critical point leading to a line of first-order LLPTs [23,27-31]. The two liquids have the same chemical composition and contain low- and high-density species forming differently bonded domains. Such LLPTs form part of the general phenomenology for a wide range of liquids [32]. These ideas have successfully explained the existence of LLPTs, but are not able to predict glass thermodynamic properties, because they view them as a result of freezing, instead of a thermodynamic transition related to the difference of enthalpy of Phase 1 and Phase 2. The LLPT at 227.5 K looks like a first-order transformation of strong glass to fragile liquid [28].

In this paper, the glass transition is viewed as having a thermodynamic origin. There are many models describing it as a true phase transformation and experimental evidence favors this interpretation. The glass transition is seen as a manifestation of critical slowing down near a second-order phase transition with the possible existence of several classes of universality [33]. A model predicting the specific heat jump is based on a percolation-type phase transition with formation of dynamical fractal structures near the percolation threshold [34-40]. Macroscopic percolating clusters formed at the glass transition have been visualized [40]. High precision measurements of third- and fifth-order, non linear dielectric susceptibilities lead to a fractal dimension $d_F=3$ for the growing transient domains [41]. An observation of structural characteristics of medium-range order with neutrons and X-rays, leads to $d_F=2.31$ [42]. Another model, entirely based on thermodynamics, predicts the specific heat jump of strong and fragile glasses and liquid-to-liquid phase transitions [1,43]. For that, the classical nucleation equation is completed by introducing the enthalpy savings $-\varepsilon_{ls}\times\Delta H_m$, $-\varepsilon_{gs}\times\Delta H_m$, and $-\Delta\varepsilon_{lg}\times\Delta H_m$, respectively, associated with the growth critical nucleus formation leading to Phase 1 and Phase 2 above T_g and Phase 3

below T_g , where ΔH_m is the melting heat [43]. The enthalpy difference $\Delta\varepsilon_{lg}\times\Delta H_m$, associated with the formation of vitreous Phase 3 below T_g , is then equal to $(\varepsilon_{ls}-\varepsilon_{gs})\times\Delta H_m$. The coefficients ε_{ls} and ε_{gs} are linear functions of $\theta^2=(T-T_m)^2/T_m^2$, as shown by studying supercooling rate maxima of liquid elements [44,45]. A positive sign of $\Delta\varepsilon_{lg}=(\varepsilon_{ls}-\varepsilon_{gs})$ above T_g and T_m at a reduced temperature θ shows that Phase 1 is favored; a negative value would indicate that it is Phase 2 [1]. The first-order transition to a glass of confined liquid helium under pressure has been described using $\varepsilon_{ls0}=\varepsilon_{gs0}=0.217$ [45]. This glass is ultrastable if there is no more enthalpy to relax in this state. These values of ε_{ls0} and ε_{gs0} , determined in many pure liquid elements at their melting temperature (T_m), correspond to the Lindemann coefficient 0.103 [46]. The transformation temperature (T_{sg}) of fragile glasses in ultrastable phases with higher density has been defined as a function of an enthalpy excess $\Delta\varepsilon\times\Delta H_m$ frozen after quenching. The denser ultrastable glass attains its lowest enthalpy at a transformation temperature T_{sg} for a value of $\Delta\varepsilon$ equal to the frozen enthalpy of the glass below T_g [5]. Phase 3 can be transformed into polyamorphous phases producing sharp enthalpy changes at various temperatures (T_{sg}) depending on smaller $\Delta\varepsilon$. The most-ultrastable phase is up to now the fully-relaxed glass.

2- Basic equations applied to water

The completed nucleation equation is given by (1):

$$\Delta G = \frac{4\pi R^3}{3} \Delta H_m / V_m \times (\theta - \varepsilon) + 4\pi R^2 (1 + \varepsilon) \sigma_1 \quad (1)$$

where ΔG is the Gibbs free energy change per volume unit, (associated with the formation of a spherical growth nucleus of radius R), ε is a fraction of the melting enthalpy ΔH_m (equal to ε_{ls} for a nucleus of Phase 1, ε_{gs} for a nucleus of Phase 2, $\Delta\varepsilon_{lg}$ for a nucleus of Phase 3), V_m is the molar volume, and $\theta=(T-T_m)/T_m$ is the reduced temperature. The melting heat ΔH_m and T_m are assumed to be the same, whatever the nucleus radius R is, and not dependent on R . The critical nucleus can give rise to Phase 1, Phase 2, glass Phase 3, or various LLPT, according to the thermal variations of ε . The new surface energy is $(1+\varepsilon)\times\sigma_1$ instead of σ_1 . The classical equation is obtained for $\varepsilon=0$ [47]. The homogeneous nucleation temperatures are $\theta_n=(\varepsilon-2)/3$ for $\theta < 0$ and $\theta_n=\varepsilon$ for $\theta > 0$ [1,43]. The critical radius is infinite at the homogeneous nucleation temperature obtained for $\theta=\varepsilon$ instead of $\theta=0$ for the classical equation. A catastrophe of nucleation occurs at $\theta=\varepsilon$ for crystals protected against surface melting [48].

The coefficients ε_{ls} and ε_{gs} in equations (2) and (3) represent values of $\varepsilon(\theta)$, and lead to the nucleus formation having the critical radius for Phase 1 and Phase 2 supercluster formations under pressure:

$$\varepsilon_{ls}(\theta) = \varepsilon_{ls0}(1 - \theta^2 \times \theta_{0m}^{-2}) + P_1, \quad (2)$$

$$\varepsilon_{gs}(\theta) = \varepsilon_{gs0}(1 - \theta^2 \times \theta_{0g}^{-2}) - \Delta\varepsilon + P_2, \quad (3)$$

where $\Delta\varepsilon$ is the coefficient of enthalpy excess in Phase 2 being frozen after quenching Phase 1; $P_1=(p-p_0)\times V_{m1}/\Delta H_m$ and $P_2=(p-p_0)\times V_{m2}/\Delta H_m$ are the contributions of the pressure (p) to the enthalpy coefficients ε_{ls} and ε_{gs} , and p_0 is the ambient pressure [5]. The coefficients ε_{ls} and ε_{gs} are equal to zero at the reduced

temperatures θ_{0m} and θ_{0g} for $\Delta\varepsilon=0$ and $P_1=0$, and they correspond to the Vogel-Fulcher-Tammann temperatures above and below T_g , respectively. Equations (2) and (3) are applicable at the homogeneous nucleation temperatures θ_{n-} in Phase 1 and Phase 2 respectively. Equation (4) determines θ_{n-} for Phase 2, combining (3) with $\theta_{n-}=(\varepsilon_{gs}-2)/3$ [43]:

$$\theta_{n-}^2 \times \varepsilon_{gs0} \times \theta_{0g}^{-2} + 3\theta_{n-} + 2 - \varepsilon_{gs0} + \Delta\varepsilon - P_2 = 0 \quad (4)$$

The solutions for θ_{n-} are given by (5):

$$\theta_{n-} = (-3 \pm [9 - 4(2 - \varepsilon_{gs0} + \Delta\varepsilon - P_2)\varepsilon_{gs0} / \theta_{0g}^2]^{1/2})\theta_{0g}^2 / (2\varepsilon_{gs0}) \quad (5)$$

θ_{n-} of Phase 2 for the sign + is called θ_2 , given by (5).

Equation (6) determines the homogeneous nucleation temperature θ_{n-} , for Phase 1, combining (2) at this temperature with $\theta_{n-}=(\varepsilon_{ls}-2)/3$:

$$\theta_{n-}^2 \times \varepsilon_{ls0} \times \theta_{0m}^{-2} + 3\theta_{n-} + 2 - \varepsilon_{ls0} - P_1 = 0 \quad (6)$$

The reduced homogeneous nucleation temperature θ_{n-} of Phase 1 under pressure in (7) is deduced from (6):

$$\theta_{n-} = (-3 \pm [9 - 4(2 - \varepsilon_{ls0} - P_1)\varepsilon_{ls0} / \theta_{0m}^2]^{1/2})\theta_{0m}^2 / (2\varepsilon_{ls0}) \quad (7)$$

θ_{n-} in (7) is called θ_1 for the sign +. The glass transition occurs at θ_g when $\varepsilon_{ls}(\theta)$ in (2) is equal to $\varepsilon_{gs}(\theta)$ in (3). θ_1 and θ_2 are equal to θ_g in strong glasses because $\varepsilon_{ls}(\theta_g)=\varepsilon_{gs}(\theta_g)$ for $\Delta\varepsilon=0$ and $P_1=P_2=0$.

As water is a strong glass at low temperatures, the coefficients ε_{gs0} in equation (8) and ε_{ls0} in equation (9), deduced from equation (4) with $P_2=0$ and from equation (6) with $P_1=0$ and $\Delta\varepsilon=0$, are determined from the knowledge of θ_g , θ_{0g} , and θ_{0m} [43]:

$$\varepsilon_{gs0} = \frac{3\theta_g + 2}{1 - \theta_g^2 / \theta_{0g}^2} \quad (8)$$

$$\varepsilon_{ls0} = \frac{3\theta_g + 2}{1 - \theta_g^2 / \theta_{0m}^2} \quad (9)$$

where the reduced temperatures θ_{0g} and θ_{0m} are equal to -1 and -2/3, respectively, because the Vogel-Fulcher Tamman temperatures are equal to 0 K below T_g and to $T_m/3$ (above T_g) for many pure, strong liquid elements [44]. With $T_g=136.6$ K, $\theta_g=-0.5$, ε_{gs0} is equal to 0.66667 and ε_{ls0} to 1.14286. The frozen enthalpy at T_g is equal to the minimum value $-0.3704 \times \Delta H_m$ of $(\varepsilon_{ls}-\varepsilon_{gs}) \times \Delta H_m$ obtained for $\varepsilon_{ls}=0$ at $\theta=\theta_{0m}=-2/3$ without imposing any entropy constraint [15]. The heat capacity jump at T_g is equal to: $(d\varepsilon_{ls}/dT-d\varepsilon_{gs}/dT) \times \Delta H_m = -1.905 \times \Delta H_m / T_m = 41.9 \text{ JK}^{-1} \text{ mole}^{-1}$ in agreement with old measurements [18], as

shown in Figure 1. The specific heat excess $\Delta C_p(T)=d(\varepsilon_{ls}-\varepsilon_{gs})/dT \times \Delta H_m$ of supercooled liquid only exists above the Kauzmann temperature because the entropy excess of supercooled liquid cannot be larger than the fusion entropy ΔS_m . $\Delta C_p(T)$ is used to evaluate the Kauzmann temperature (T_K) of supercooled water. The entropy excess (ΔS_m) of supercooled water is equal to $\Delta H_m/T_m=6000/273.1=22 \text{ J.K}^{-1}\text{mole}^{-1}$ between 227.5 K and $T=116.5$ K and between 119.7 K and 273.1K. The Kauzmann temperature occurs at $T_K \cong 116.5 \text{ K}-119.7 \text{ K}$.

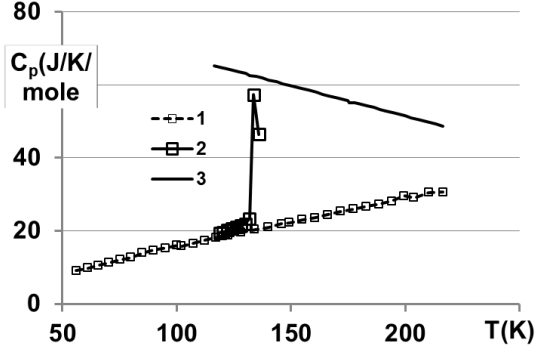


Figure 1: 1. Heat capacity of hexagonal ice [18] 2. Heat capacity jump at 133.6 K [18]; 3. Supercooled water heat capacity calculated with the derivative $(d\varepsilon_{ls}/dT-d\varepsilon_{gs}/dT) \times \Delta H_m$.

For confined supercooled water in pores of radius $R=0.55 \text{ nm}$ [21,22], θ_2 is equal to -0.167 (227.5 K) for $P_2=0.8505$ and $\Delta\varepsilon=0$ in equation (5). Using the Young-Laplace equation, Δp is equal to $2\gamma/R=0.31 \pm 0.02 \text{ GPa}$, with a value of the surface tension $\gamma=0.085 \pm 0.005 \text{ J/m}^2$ at 227.5 K, extrapolated from its thermal variation above 250 K [23]. The enthalpy coefficient (P_2) is deduced to be close to 0.8505 with $V_{m2} \cong 16.5 \times 10^{-6} \text{ m}^3$ and $p=0.31 \text{ GPa}$.

The enthalpy difference coefficient $\Delta\varepsilon_{ig}$ between vitreous Phase 3 and liquid Phase 1 is given by equation (10) under pressure (p):

$$\Delta\varepsilon_{ig}(\theta) = (\varepsilon_{ls} - \varepsilon_{gs}) = \varepsilon_{ls0} - \varepsilon_{gs0} + \Delta\varepsilon + P_1 - P_2 - \theta^2 \left(\frac{\varepsilon_{ls0}}{\theta_{0m}^2} - \frac{\varepsilon_{gs0}}{\theta_{0g}^2} \right) \quad (10)$$

The difference $\Delta P=(P_1-P_2)=\delta V \times p/\Delta H_m$ is proportional to the volume change (δV), and to the pressure (p) at the transformation temperature (θ). (ΔP) is equal to zero for $\delta V=0$ in the absence of latent heat. The homogeneous nucleation temperature of Phase 3 also occurs for $\Delta\varepsilon_{ig}=0$ with $\Delta\varepsilon=0$ because Phase 1 and Phase 2 have the same homogeneous nucleation temperature $\theta_1=\theta_2=\theta_g$.

A sharp enthalpy difference between non-relaxed glass Phase 3 and fully-relaxed glass Phase 3 can be induced in all glasses below T_g for $\Delta\varepsilon_{ig}=0$ in (10), when an enthalpy excess coefficient ($\Delta\varepsilon$) exists after rapid cooling, as already described for an ultrastable glass formation [5,10]. This enthalpy difference is equal to $-2 \times \Delta\varepsilon_{ig}(\theta) \times \Delta H_m$ above θ_K for $\Delta\varepsilon=0$ and $P_1=P_2=0$ because it cannot exceed the frozen enthalpy which is available at any temperature below T_g . This transformation temperature T_{sg} for a stable glass formation given in (11) is equal to, or larger than, T_K and is also induced by pressure. It depends on δV and on the value of $\Delta\varepsilon$ at this temperature.

$$\theta_{sg} = - \left[(\varepsilon_{ls0} - \varepsilon_{gs0} + \Delta\varepsilon + \Delta P) / (\varepsilon_{ls0}\theta_{0m}^{-2} - \varepsilon_{gs0}\theta_{0g}^{-2}) \right]^{1/2} \quad (11)$$

After decompression, the enthalpy change coefficients of supercooled water are represented in Figure 2. The line $\Delta\varepsilon_{lg}=0$ at the origin corresponds to a quenched glass phase, containing a positive enthalpy excess which is equal to $\Delta\varepsilon \times \Delta H_m = [-1.14286 \times (1 - 2.25 \times \theta^2) + 0.66667 \times (1 - \theta^2)] \times \Delta H_m$ above the line 1 because $\Delta\varepsilon_{lg}$ of the glass phase is negative for $\Delta\varepsilon=0$. The total enthalpy of this quenched phase is then equal to that of Phase 1. The nonrelaxed glass phase is represented by Line 1 and the fully-relaxed phase at thermodynamic equilibrium by Line 2. A sharp, spontaneous transition is observed at 117 K during heating of the HDA phase [10] and this corresponds to an enthalpy coefficient excess $\Delta\varepsilon=0.146$ at $\theta=-0.5735$ as shown in Figure 2. The latent heat measured using continuous heating is $757 \pm 144 \text{ J.mole}^{-1}$ [6] and it corresponds to the relaxation of an enthalpy excess equal to $0.146 \times \Delta H_m = 876 \text{ J.mole}^{-1}$. An isothermal relaxation at $T_{sg}=117 \text{ K}$ would have to deliver a latent heat two times larger (and equal to 1752 J.mole^{-1}) as shown in Figure 2. The sample volumes of HDA in Figure 3 have been also measured at $p=0$ after a duration of about 3 hours of isotherm annealing [10]. In these conditions, a sharp volume change of $0.16 \times 10^{-6} \text{ m}^3 \text{ g}^{-1}$ occurs at $115 \pm 0.5 \text{ K}$ confirming the existence of spontaneous and high enthalpy relaxation of about 1752 J.mole^{-1} from HDA to LDA phases. Following this analysis, this transition temperature at T_{sg} is the first observation of a glass Kauzmann temperature (T_K) because spontaneous and sharp enthalpy relaxation is only possible above T_K . Latent heats are still produced at various temperatures (T_{sg}) depending on $\Delta\varepsilon$ and they correspond to partial relaxations of Phase 3. This type of transition has already been observed in other glasses obtained by vapour deposition on substrates maintained at the temperature T_{sg} using very slow deposition rates [2,4] and described by the same model [5]. This analysis is based on the existence of two main glass phases (Phase 3), the first one being the nonrelaxed classical glass phase with its frozen enthalpy equal to $-0.37037 \times \Delta H_m$ and the second one the ultrastable glass phase which is expected to be fully relaxed with a maximum enthalpy reduction equal to $-0.2923 \times \Delta H_m$ (at approximately $T_K \cong 117 \text{ K}$).

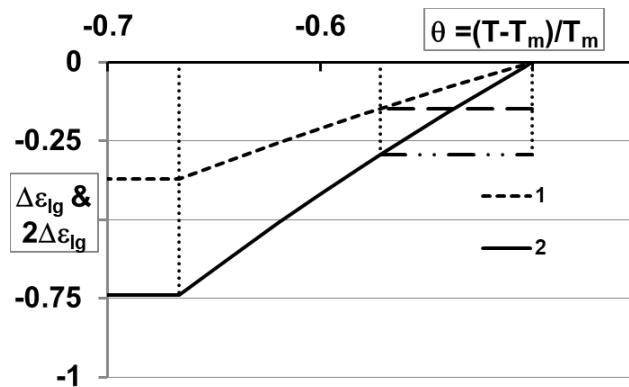


Figure 2: Prediction of reduced temperatures θ_{sg} along the line $\Delta\varepsilon_{lg}=0$ and latent heat coefficients $\Delta\varepsilon_{lg}$ associated with the glass-to-glass transformations at zero pressure. Lines numbered from 1 to 2: 1. $\Delta\varepsilon_{lg}(\theta)$ given by equation (10) of nonrelaxed Phase 3 with $\Delta\varepsilon=0$, $\Delta P=0$, $\theta_g=-0.5$ ($T_g=136.6 \text{ K}$); 2. Equilibrium enthalpy coefficient $2 \times \Delta\varepsilon_{lg}(\theta)$ of fully-relaxed Phase 3 crossing $\theta_g=-0.5$ ($T_g=136.6 \text{ K}$). Observed reduced

temperature $\theta_{sg}=-0.5735$, corresponding to $T_{sg}=T_K\cong 117$ K, accompanied by latent heats equal to 877J.mole^{-1} ($\Delta\varepsilon_{ig}=-0.14615$) or 1752J.mole^{-1} ($2\times\Delta\varepsilon_{ig}=-2\times 0.14615=-0.2923$).

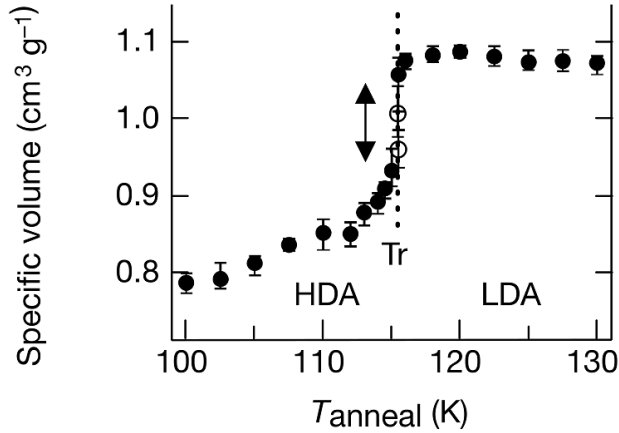


Figure 3: Reproduced from [10] with Nature Publishing Group permission. Isotherm annealing of HDA at different temperatures over 3 hours' duration. Specific volume versus annealing temperature.

Sharp, exothermic latent heats are still observed in water after decompression of VHDA at 77K from various pressures, see Figure 4 [20]. VHDA under pressure has a much larger density than HDA. The glass transition at 136.6 K and after decompression is not detected in these samples (Figure 4). The sharp, exothermic latent heats observed below 136 K decrease the density and give rise to ice which contains orientational disorder instead of fully relaxed Phase 3 [49]. The latent heat at the crystallization temperature of 164 K seems to depend on the preceding exothermic heat. The absence of glass transition at 136.6 K confirms that the sharp transitions of polyamorphous phases at $p=0$ [20] lead to amorphous ice resulting from molecular reorientation processes [49]. The enthalpy coefficient along Line 2 in Figure 2 cannot be attained without amorphous ice formation. Sharp exothermic latent heats are observed around $T_{sg}=125, 126, 130, 132, 134$ K and predicted to be equal along Line 2 to 1000, 876, 562, 383, 217 J.mole^{-1} respectively. The latent heats at 130, 132, and 134 K are in rough agreement with those observed in Figure 4, whereas those at 125 and 126.5 K are smaller because the annealing time at these temperatures is too small during a continuous heating.

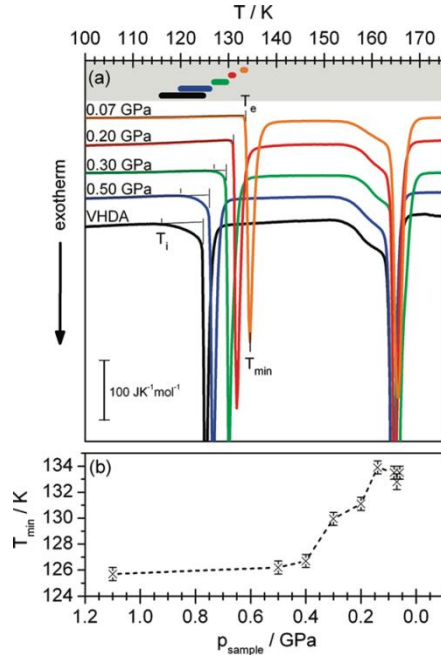


Figure 4: Reprinted from [20, Figure 3] with ACS permission . “ (a) DSC scans recorded at a rate of 10 K/min. The DSC output signal was normalized to 1 mol. The samples were heated from 93 to 253 K; thermograms are plotted in the temperature range of 100–175 K. Shown are VHDA (black line) and four samples made by decompression of VHDA at 140 K to 0.5 (blue line), 0.3 (green line), 0.2 (red line), and 0.07 GPa (orange line). First exothermic peak: transition to LDA; second exothermic peak: crystallization to cubic ice. The bars in the top part indicate the difference between T_i and T_e , which is a measure of the relaxation state of the sample. (b) The temperature at the peak minimum T_{min} is shown as a function of the pressure from which the sample has been recovered. The values are not only obtained from the four selected runs depicted in (a) but represent mean values obtained from several runs” There is no detectable endothermic event at $T=136.6$ K.

There are two regions of water crystallization (at approximately 230–250 K and 135–165K) confirming the existence of a LLPT between this two regions in all the samples studied. Supercooled water undergoes a first-order phase transition that separates fragile from strong states. Fragile liquids have values of ε_{ls0} given in (12) [43]:

$$\varepsilon_{ls}(\theta = 0) = \varepsilon_{ls0} + P_1 = 1.5 \times \theta_1 + 2 + P_1 = a \times \theta_g + 2 + P_1, \quad (12)$$

where $a=1$ leads to a specific heat excess $\Delta C_p(T)$ of the supercooled melt at the glass transition equal to $1.5 \times \Delta H_m / T_m$ [50-52]. The reduced temperature θ_{0m} is given by (13), and is a double solution for (6):

$$\theta_{0m}^2 = \frac{8}{9} \varepsilon_{ls0} - \frac{4}{9} \varepsilon_{ls0}^2. \quad (13)$$

New parameters ε_{gs0} and θ_{0g} are fixed at T_g and below T_g in equations (14) and (15) to give a double solution for (4) with $a=1$ because $a < 1$ leads to a too high nucleation temperature (T_1) in Phase 1; ε_{gs0} is maximized by (14) and (15) [43]:

$$\varepsilon_{gs}(\theta = 0) = \varepsilon_{gs0} + P_2 = 1.5 \times \theta_g + 2 + P_2, \quad (14)$$

$$\theta_{0g}^2 = \frac{8}{9} \varepsilon_{gs0} - \frac{4}{9} \varepsilon_{gs0}^2. \quad (15)$$

The first-order transition under Laplace pressure of fragile-to-strong water in confined space, occurs at $T_{LL}=227.5$ K, $\theta_{LL}=-0.167$, and $T_m=273.1$ K for the melting temperature of superclusters percolating in the glass state as assumed in equation (1) [22]. The two temperatures, where $\Delta\varepsilon_{lg}$ in equation (10) is equal to zero, cannot depend on the pressure because there is no volume change there. In the fragile state of water, these two reduced temperatures are $\theta_{LL}=\pm 0.16705$ and they are symmetrical with regard to T_m in Figure 5. For $\Delta\varepsilon_{lg}=0$ above T_m , there is a compressibility minimum of bulk water at 45.6°C because Phase 2 replaces Phase 1 without volume change at this temperature as shown in Figure 5 [23,53,54]. Then, the first-order transition of fragile-to-strong liquid does not depend on the pressure at $\theta_{LL}=-0.167$. The value $a=1$ used in Figure 5 leads to $\varepsilon_{is0}=1.7953$, $\varepsilon_{gs0}=1.69295$, $\theta_{0g}^2=0.23103$, $\theta_{0m}^2=0.16333$ with $\theta_g=-0.2047$ and to $T_l=235.9$ K in good agreement with a maximum supercooling of water equal to 35 K. The coefficients ε_{is} and ε_{gs} of fragile liquids are equal to 1.5 at $\theta=\theta_{LL}$ while ε_{is} and $\Delta\varepsilon_{lg}$ of strong liquids are respectively equal to 1.07102 and 0.42298. Under these conditions, the water specific heat increase up to $81 \text{ J.K}^{-1} \text{ mole}^{-1}$ at $\theta_{LL}=-0.167$ [22], is due to an LLPT [23,27-30]. This increase is not only observed at zero pressure, but also under a Laplace pressure of 0.31 ± 0.02 GPa in 1.1 nm pores, slightly increasing with decreasing temperature [22,55-57]. In Figure 5, the LLPT at 227.5 K and zero pressure is accompanied (during heating) by an exothermic latent heat of $(-1.5+1.07102+0.42298)\times\Delta H_m=-0.006\times\Delta H_m$ associated with Phase 1 and Phase 3 transformations because glass Phase 3 is transformed in liquid Phase 3 at T_g and continues to exist as a liquid phase above T_g . As expected [22-28], a critical point seems to exist for $p=0$ in these conditions.

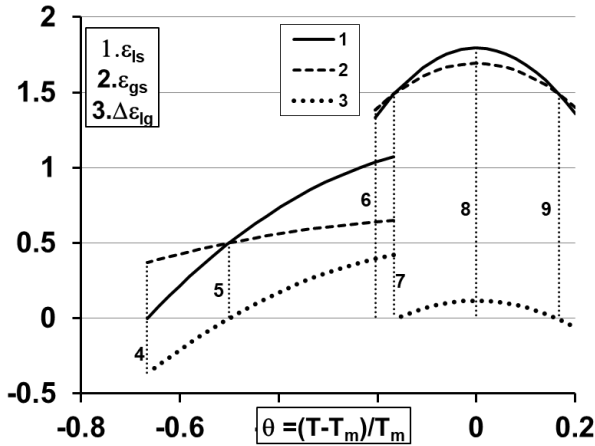


Figure 5: The enthalpy coefficients ε_{is} , ε_{gs} and $\Delta\varepsilon_{lg}$ of Phase 1, Phase 2 and Phase 3, $P=0$. For the strong liquids at $\theta_{LL}=-0.167$, $\varepsilon_{is} = 1.07102$, $\varepsilon_{gs} = 0.64804$, $\Delta\varepsilon_{lg} = 0.42298$ and at $\theta_g = -0.5$, $\varepsilon_{is} = \varepsilon_{gs} = 0.5$. For the fragile liquids at $\theta_{LL}=-0.167$, $\varepsilon_{is} = \varepsilon_{gs} = 1.5$. Curves numbered from 1 to 3: 1- $\varepsilon_{is}(\theta)$ of Phase 1 given by (2) below $\theta_{LL}=-0.167$ in the strong water and above in the fragile one; 2- $\varepsilon_{gs}(\theta)$ of Phase 2 given by (3) below and above $\theta_{LL}=-0.167$; 3- $\Delta\varepsilon_{lg}(\theta)$ of Phase 3 below and above θ_{LL} . Temperatures numbered from 4 to 9: 4- The frozen enthalpy coefficient $\Delta\varepsilon_{lg}$ equal to -0.3704 at $\theta=-2/3$; 5- The glass transition $\theta_g=-0.5$ ($T_g=136.6$ K); 6- $\theta_g=-0.2047$ of the fragile water in the absence of LLTP; 7- At $\theta_{LL}=-0.167$, $T_{LL}=227.5$ K,

the LLTP for $\Delta\varepsilon_{lg}=0$; 8- $\theta=0$ the melting temperature at $T_m=273.14$ K; 9- For $\theta=0.167$, $\Delta\varepsilon_{lg}=0$ at the isothermal compressibility minimum temperature 318.7K.

3- First-order transformations LDA-HDA under pressure

High pressure applied to ice samples followed by complete decompression, induces an LDA phase which has a density and, consequently, an enthalpy close to that of ice [6]. The LDA phase is viewed as having an enthalpy difference of $-0.3704 \times \Delta H_m$ with that of the glass phase at all temperatures $T < T_g$. The LDA to HDA involving high pressures and an enthalpy excess ($\Delta\varepsilon$) due to Phase 1 quenching is frozen because the melting temperature (T_m) is strongly decreased, and the sample is cooled during decompression from temperatures much higher than T_m . In Figure 6, compression experiments of this LDA phase at various temperatures, transform it into an HDA phase at a well-defined pressure (p). This sharp transformation is also viewed as an HDA to LDA transformation because this first-order transition is reversible at T_{sg} . The volume change δV in (10) does not depend on the pressure (p) and is equal to $0.2 \times 10^{-6} \text{ m}^3 \text{ g}^{-1}$, as shown in Figure 6 [8].

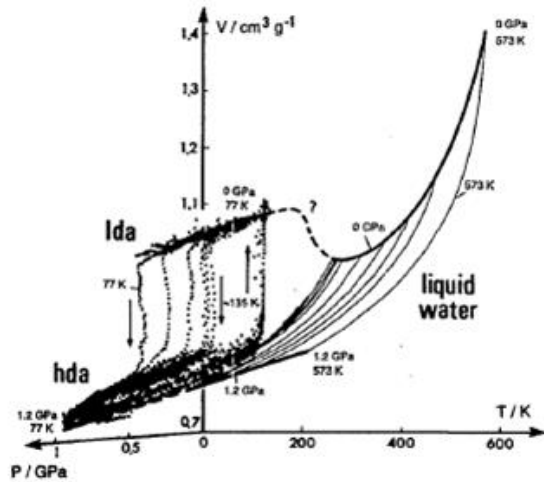


Figure 6: Specific volume versus pressure (GPa) and Temperature (K). Reprinted from [8, Figure 4] with AIP permission. “Low density amorphous to high density amorphous transformations under pressure occur for $p=0.55, 0.45, 0.38, 0.32, 0.05$ GPa and $T=77, 100, 121, 135, 140$ K respectively. Liquid water under 1.2 GPa and 0 pressures is also represented versus temperature. The linkage between LDA and liquid state at zero pressure occurs at 227 K. The liquid at zero pressure corresponds to Phase 1”

All values of various quantities are given in Table 1. The sharp enthalpy changes under pressure (p) are equal to $\Delta P_2 = 0.3704 \times \Delta H_m$ and occur at $\theta = \theta_{sg}$, as given by equation (11). LDA is viewed as having the enthalpy of nonrelaxed glass Phase 3 and an effective enthalpy excess $\Delta\varepsilon_{eff}$, and it is expected to have an enthalpy difference $-\Delta P_2$ with HDA for $T_{sg} < T < T_g$. This LDA-HDA first-order transformation is subject to an enthalpy constraint setting that the total enthalpy increase at equilibrium cannot be larger than the maximum frozen enthalpy $0.3704 \times \Delta H_m$ (produced at $\theta = -2/3$). In Figure 7, the values of $\Delta\varepsilon_{eff} = \Delta\varepsilon + \Delta P_1$ given in Table 1 (obtained using (10) for $\theta = \theta_{sg}$ and represented as a function of θ_{sg}^2), depend on pressure

via ΔP_1 which is the initial enthalpy change under pressure associated with the glass volume change below T_g , before the occurrence of the first-order transition. The values of $\Delta \varepsilon_{\text{eff}}$ at the temperature θ_{sg} are negative because ΔP_1 is negative. The enthalpy excess $\Delta \varepsilon$, in the absence of pressure, is equal to $(-\varepsilon_{\text{lg}} + \varepsilon_{\text{gs}})$ and varies from 0.3704 at $T=77$ K to zero at 136.6 K, as shown in Table 1. Enthalpy excess depends on the reduced temperature θ below 136.6 K, as has already been observed in hyperquenched glasses below T_g [58-60]. The values of ΔP_1 are deduced from the difference: $\Delta \varepsilon_{\text{eff}} - \Delta \varepsilon$. The melting temperatures (T_m) under pressure are assumed to be those of hexagonal ice [9]. They lead in water to the maximum change of the enthalpy coefficient $\Delta \varepsilon_{\text{lg}} = 0.3704$ at the transformation temperature T_{sg} and for $0.31 < p \leq 0.6$ GPa. The first-order transformation of LDA-HDA, takes into account the entropy constraint which could not be respected for an enthalpy relaxation.

Table 1: 1- p the applied pressure. 2- T_{sg} the temperature of the first-order glass-to-glass transition. 3- T_m the melting temperature depending on pressure. 4- $\Delta \varepsilon$ the enthalpy excess coefficient induced by quenching at T_{sg} . 5- $\Delta P_1 = p \times \delta V_1 / \Delta H_m$ the change of the enthalpy coefficient associated with the volume difference between liquid and glass just before the transformation from LDA to HDA under pressure (p); ΔH_m the fusion heat. 6- $\theta_{\text{sg}} = (T_{\text{sg}} - T_m) / T_m$. 7- $\Delta P_2 = p \times \delta V_2 / \Delta H_m$ the change of the enthalpy coefficient associated with the volume difference induced by the first-order transition under pressure. 8- $\Delta \varepsilon_{\text{eff}} = \Delta P_1 + \Delta \varepsilon$ the effective enthalpy excess coefficient under pressure. 9- $\theta_g = (T_g - T_m) / T_m$ the reduced glass transition temperature of HDA under pressure p . 10- f the HDA entropy fraction from T_{sg} to T_g under pressure (p). 11- ΔS the entropy excess under pressure of HDA from T_g to T_m . 12- θ_{gs} the reduced glass transition temperature of HDA under pressure calculated from the entropy constraint. 13- T_{gs} the glass transition temperature of HDA under pressure deduced from the entropy constraint. 14- T_g the glass transition temperature calculated from equation (5) assuming the enthalpy coefficient difference of HDA with LDA is $(\varepsilon_{\text{gs}0} + \Delta P_2) = 0.66667 + 0.3704 = 1.037$ instead of $\varepsilon_{\text{gs}0}$ for $p=0$.

1	p (GPa)	0.6	0.5	0.42	0.35
2	T_{sg} (K)	77	100	121	135
3	T_m (K)	154	186	215	229
4	Δε	0.3704	0.2892	0.1148	0
5	ΔP₁	-0.3704	-0.3582	-0.2295	-0.1654
6	θ_{sg}	-0.5	-0.4624	-0.4372	-0.4035
7	ΔP₂	0.3704	0.3704	0.3704	0.3704
8	Δε_{eff}	0	-0.067	-0.111	-0.154
No man's land					
9	θ_g	-0.3677	-0.3677	-0.3677	-0.3677
10	f=0.3704×T_m/T_{sg}	0.741	0.689	0.658	0.621
11	ΔS(JK⁻¹mol⁻¹)	5.7	6.84	7.52	8.34
12	θ_{gs}	-0.325	-0.352	-0.366	-0.383
13	T_{gs} (K)	104	121	136	141.3
14	T_g (K)	97.4	117.6	136	144.7

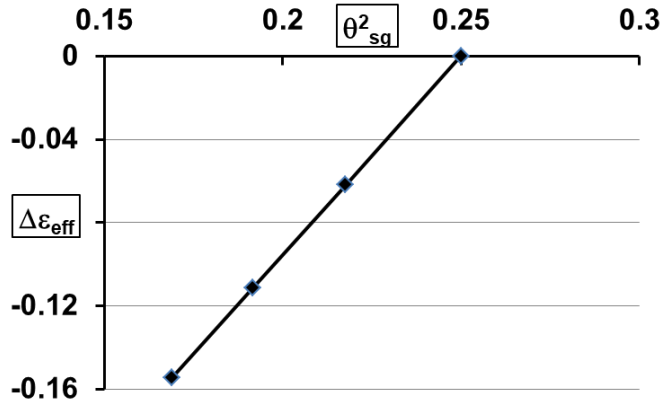


Figure 7: $\Delta\epsilon_{eff}$ versus θ_{sg}^2 . The values of $\Delta\epsilon_{eff}$ and θ_{sg} are reported in Table 1.

In Figure 8, the transformation under pressure starts from Line 3 and leads to HDA, including $\Delta\epsilon_{eff}$ on line 1 which is characterized by an enthalpy increase equal to the frozen enthalpy ($0.3704 \times \Delta H_m$) below $T_g = 136.6$ K. The volume change ($\delta V = 0.3704 \times \Delta H_m / 18 / p = 0.206 \times 10^{-6} \text{ m}^3 \text{ g}^{-1} \text{ GPa}^{-1}$ for $p = 0.6$ GPa) is constant under various pressures (p), and equal to the experimental value presented in Figure 6. The enthalpy difference coefficient ($\Delta P_2 = -0.3704$) is the sum of $\Delta\epsilon_{eff}$ and ΔP_1 . ΔP_1 is negative and proportional to the applied pressure in agreement with Figure 6. The slope $d\Delta\epsilon_{eff}/dp$ corresponds to the measured value ($dV/dp = 0.21 \text{ g}^{-1} \text{ cm}^3 \text{ GPa}^{-1}$) of the LDA phase [13, Figure 14].

The LDA-to-HDA transformation, occurring for $p = 0.35$ GPa in the interval 130–140 K, is reversible when the pressure is decreased down to $p = 0.05$ GPa [8]. This reversibility still proves its first-order character. The enthalpy change induced at T_{sg} is recovered near $T_g \cong 0.5 \times T_m$ after decompression down to 0.05 GPa. The enthalpy excess ($\Delta\epsilon_{eff} \times \Delta H_m$) is fully recovered at $T = T_{sg}$ and $p = 0$ because the pressure changes the enthalpy from Line 1 to Line 3, in Figure 8, and decreases the volume by a constant quantity which is recovered after decompression.

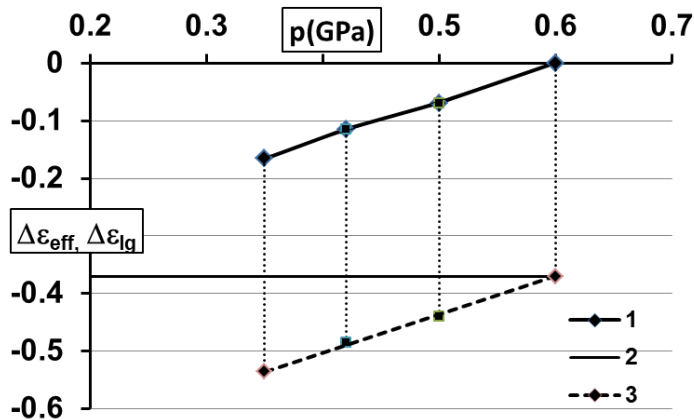


Figure 8: Enthalpy excess coefficients $\Delta\varepsilon_{\text{eff}}$ versus pressure p and sharp enthalpy coefficient changes $\Delta\varepsilon_{\text{lg}}$ at $\theta=\theta_{\text{sg}}$: 1- The line 1 is the HDA line represented by $\Delta\varepsilon_{\text{eff}}$ versus p (GPa). 2- The line 2 represents the change $\Delta\varepsilon_{\text{lg}}=-0.3704=\Delta P_2$ which is equal to $\Delta\varepsilon_{\text{eff}}+\Delta P_1$ given in Table 1. ΔP_1 is proportional to p . 3- The line 3 is the LDA line with a slope corresponding to $dV/dp=0.206\text{ g}^{-1}\text{cm}^3\text{GPa}^{-1}$. Calculated points roughly correspond to Mishima's measurements reproduced in Figure 6 at $T=77\text{K}$ for $p=0.6\text{ GPa}$ instead of 0.55 GPa , for $p=0.5$ instead of 0.45 GPa , for $p=0.42$ instead of 0.38 GPa , and for $p=0.35\text{ GPa}$ instead of 0.32 GPa [8].

A relaxation of the enthalpy excess $\Delta\varepsilon$ has been observed [22] for water confined into 1.1nm pores being submitted to Laplace pressure and this is reproduced in Figure 9. "The systematic heat-evolution and heat-absorption effects for the rapidly and slowly cooled samples are characteristic of a glass transition, and two transitions are found" between the ranges 124-136 K and 163-172 K. The glass transition of all LDA phases above T_{sg} is given by (5) where $\Delta\varepsilon-P_2=0$ and ε_{gs0} is replaced by $\varepsilon_{\text{gs0}}+\Delta P_2=0.66667+0.37034=1.037$ because ΔP_2 results from the first-order transition at T_{sg} instead of relaxation. It is equal to $\theta_{\text{g}}=-0.3677$ and $T_{\text{g}}=0.632\times T_{\text{m}}$. With $T_{\text{m}}=273.1\text{ K}$, the T_{g} of confined water is expected to occur at 173 K. $\Delta\varepsilon=-\Delta\varepsilon_{\text{lg}}$ disappears at $\theta_{\text{g}}=-0.5$ ($T_{\text{g}}=136.6\text{ K}$) when $\Delta\varepsilon_{\text{lg}}=0$. The relation $\Delta\varepsilon_{\text{eff}}=\Delta\varepsilon+\Delta P_1$ shows that $\Delta\varepsilon_{\text{eff}}=\Delta P_1$ occurs at $T\cong 136.6\text{ K}$. This equality occurs in Figure 9 for $\Delta P_1=-0.3704/2=-0.185$. The Laplace pressure at $T\cong 136\text{ K}$ is then equal to 0.30 GPa in good agreement with 0.31 GPa at $T_{\text{LL}}=227.5\text{K}$.

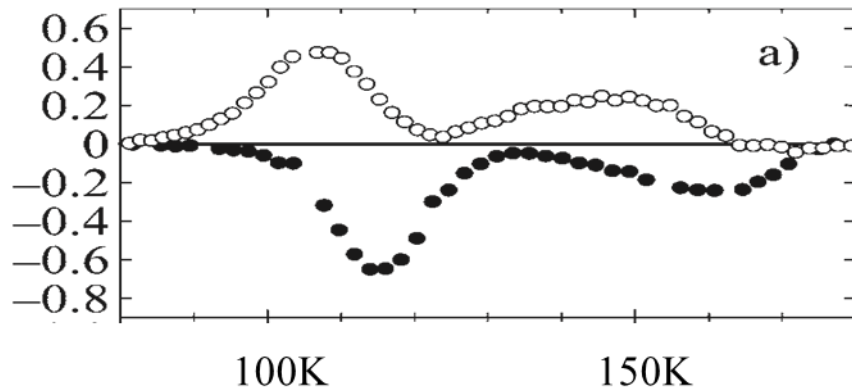


Figure 9: Reproduced from [22] with AIP permission. "Temperature dependence of the rates of spontaneous heat release and absorption, observed in the heat-capacity measurements of ordinary water (H_2O) by an intermittent heating method. Average pore diameter: a) 1.1 nm, ○=sample cooled rapidly at around $5\text{ K}\cdot\text{min}^{-1}$ before the measurements, ●=sample cooled slowly at $10\text{ mK}\cdot\text{min}^{-1}$ ".

The glass transition calculated by equation (5) occurs where $\theta_{\text{g}}=-0.5$ ($T_{\text{g}}=0.5\times T_{\text{m}}$) at low pressures in the absence of an LDA-HDA transition. The HDA phase has a larger enthalpy, and the new glass transition temperature of HDA is still equal to (5) and $T_{\text{g}}=0.632\times T_{\text{m}}$ depending on the melting temperature (T_{m}) under pressure. For $p=0.6\text{ MPa}$, $T_{\text{m}}=154\text{ K}$, $T_{\text{g}}\cong 97.4\text{ K}$; for confined water in 1.1 nm pores, $T_{\text{g}}=173\text{ K}$ which is in agreement with Figure 9.

The first-order LDA-HDA transition at T_{sg} under pressure is accompanied by an entropy change equal to $0.3704 \times \Delta H_m / T_{sg} = f \times \Delta H_m / T_m$ where f is a fraction of the fusion entropy at the melting temperature under pressure which is recovered at the glass transition, T_{gs} :

$$f = 0.3704 \times T_m / T_{sg} \quad (16)$$

Values for f are given in Table 1. The entropy (ΔS) of HDA at T_{gs} in Table 1 is counted from T_{gs} to the melting temperature T_m using the specific heat, deduced from $d\Delta\epsilon_{lg}/dT$, because the LLPT has disappeared above $p=0.31$ GPa (see section 3). Some glass transitions (under a pressure at θ_{gs} and T_{gs} calculated using the entropy constraint) are given in Table 1 and they roughly equate to the calculated values θ_g and T_g using equation (5). The uncertainty on ΔS values is estimated to be 8.6% from the difference between $\Delta S=7.59 \text{ J.K}^{-1}\text{mole}^{-1}$ at θ_g and $\Delta S=5.7 \text{ J.K}^{-1}\text{mole}^{-1}$ for $p=0.6$ GPa.

The first-order transition of HDA to LDA induces an enthalpy decrease equal to $-0.37037 \times \Delta H_m$ and then a very stable glass state up to $T_g=136.6$ K. In addition, a spontaneous enthalpy relaxation of this state is observed at, or above, T_K in order to attain the enthalpy of the ultrastable state after isothermal and complete relaxation of the frozen enthalpy at $T_{sg}=T_K$. This complete relaxation gives rise to orientational disorder in ice instead of ultrastable glass phase [49].

Recent studies have reported on in-situ structural characterization of LDA after decompression and relaxation between 96K and 160K by synchrotron x-ray diffraction [61]. An intermediate crystalline phase at 100K, prior to complete amorphization at 133K is observed. These results show that LDA exists under various forms depending on the relaxation temperature because any phase having a fusion entropy smaller than $\Delta H_m / T_m = 6000/273.1 = 22 \text{ J.K}^{-1}\text{mole}^{-1}$ can be condensed at a temperature equal or larger than its own Kauzmann temperature. Another publication classifies HDA as a “derailed” state along the ice Ih to high-density ice IV pathway [62]. These two papers show that the same volume changes that characterise LDA and HDA lead to various phases including “derailed” states depending on relaxation time and temperature before attaining ice. Nevertheless, relaxed LDA has an enthalpy still smaller than that already frozen below T_g . Its enthalpy is so close to that of ice that its vitreous state can be transformed, by relaxation, through various “derailed” states on the pathway leading to the formation of ice [49].

4- The water phase diagram and the critical points under pressure

There is no more first-order transition at a critical point. By applying equations (2) and (3) and assuming $\Delta\epsilon=0$, and $P_1-P_2=0$, Lines 1 and 2 at a critical point in Figure 5 are shifted by $P=P_1=P_2$ under pressure. In Figure 10, the LLPT line, $\theta_{LL}=-0.167$ ($T_{LL}=0.832 \times T_m$), extends from $P=-0.5000$ to $P=0.8505$. A reduced temperature is used because it reduces the figure number and it may apply to the melting temperature of any ice phase.

The critical points are determined assuming that glass Phase 3 continues to exist as a liquid phase when heated above θ_g . A complementary volume change, corresponding to the HDA-VHDA transformation is observed at 125 K under higher pressures (approximately $p=0.95$ GPa) [11, Figure 1]. and is frozen after decompression at 77 K and equal to $0.0855 \text{ m}^3\text{g}^{-1}$. This transition is due to superheating of Phase 3 which disappears at the second homogeneous nucleation temperature when $\theta_{n+}=\Delta\epsilon_{lg}=1.302 \times T_m$ and it is accompanied by an enthalpy increase equal to $0.302 \times \Delta H_m = 1812 \text{ J.g}^{-1}\text{mole}^{-1}$ in the strong liquid

and a volume change $\delta V=1812/18/p=10^{-6} \text{m}^3 \text{g}^{-1}$ (which agrees with [11]). Equation (17) gives the value of θ_{n+} for all glass phases as a function of their initial enthalpy coefficient [1]:

$$\theta_{n+} = \frac{-1 + (1 + 4(\varepsilon_{ls0} - \varepsilon_{gs0} + \Delta P)(\varepsilon_{ls0}\theta_{0m}^{-2} - \varepsilon_{gs0}\theta_{0g}^{-2}))^{1/2}}{2(\varepsilon_{ls0}\theta_{0m}^{-2} - \varepsilon_{gs0}\theta_{0g}^{-2})} \quad (17)$$

where $\varepsilon_{ls0}=1.14286$, $\varepsilon_{gs0}=0.66667$, $\theta_{0g}=-1$, $\theta_{0m}=-2/3$ and $\Delta P=-0.3704$ for LDA.

The melting temperature (T_m) of ice, Ih, under 0.95GPa is deduced to be equal to $125/1.302=96\text{K}$ which is in agreement with Mishima's measurements [9]. The existence of a melting temperature above T_m due to Phase 3 superheating suggests that any liquid Phase 3 is "ordered" above T_g and T_m . The existence of an "ordered liquid" state has already been suggested to exist above T_g and above T_m in $\text{Zr}_{41.2}\text{Ti}_{13.8}\text{Cu}_{12.5}\text{Ni}_{10}\text{Be}_{22.5}$ [63,64]. The temperature T_{n+} is observed from 1090 to 1150 K and equation (17) predicts 1116K [1]. An other glass-forming melt ($\text{Zr}_{58.5}\text{Cu}_{15.6}\text{Ni}_{12.8}\text{Al}_{10.3}\text{Nb}_{2.8}$) is ordered below 850K. Its glass transition temperature is 700 K and $T_m=1125$ K. Using equation (12) and $a=1$ because $\Delta C_p(T_g)=1.5 \times \Delta H_m/T_m$, $\theta_g=-0.378$, $\varepsilon_{ls0}=\theta_g+2=1.622$ and $1.5 \times \theta_1=\theta_g$; the homogeneous nucleation temperature T_1 in Phase 1 is calculated to be equal to 842 K. A specific heat peak is observed in Figure 11 at this temperature which shows that liquid Phase 1 is ordered below its homogeneous nucleation temperature [65]. The reference of the specific heat data is [66].

There is no more first-order transition above $P=0.8505$ because the homogeneous nucleation temperatures of strong Phase 1 and Phase 2, calculated using equations (5) and (7), reappear above θ_{LL} as shown in Figure 10.

Another point without first-order transition occurs for $P_1=0.006$ because the sum of latent heats of Phase 1 and Phase 3 at θ_{LL} is nearly equal to zero, as seen in Figure 5. These two points occur for $p_2/\rho_2=283.5$ and $p_1/\rho_1=2$ where ρ is the density in Kg.m^{-3} and p the pressure in Pascal. The pressure p_1 is equal to 18.3 MPa, where $\rho_1=915$ and $p_2=0.31$ GPa where $\rho_2=1093$ which is in rough agreement with other calculations [23,27,29,30] and with density measurements under pressure [67-69]. Liquid Phase 3 exists above T_g and this explains the presence of a point at a low pressure equal to approximately 18.3MPa where the first-order transition disappears without being the end of the first-order transition line. The corresponding pressure slightly depends on the initial choice of T_g but, it is equal to approximately $P=0$ for $T_g=135$ K instead of 136.6 K.

The specific heat increase at zero pressure below T_m proves that the LLPT is always present for $P<0.006$ and exists at negative pressures down to $P=-0.500$. Phase 3 disappears with the glass transition for $P=-0.500$ when Line 1 and Line 2 in Figure 5 are shifted by -0.500 . This third point is critical because it corresponds to the other extremity of the first-order transition line and confirms that the stability limit of the two metastable water phases occurs for $p=-175$ MPa assuming a density $\rho=950$ Kg.m^{-3} [70]. This last critical point also corresponds in Figure 5 to the highest exothermic enthalpy under pressure and then, to the maximum density at negative pressure [70,71]. When assuming zero pressure, equations (2), (3), and (10) indicate that the first-order transformation during heating could be endothermic between $P=0.006$ and $P=0.8505$ and exothermic for $-0.5<P<0.006$ adding Phase 1 and Phase 3 contributions to the latent heat (see Figure 5).

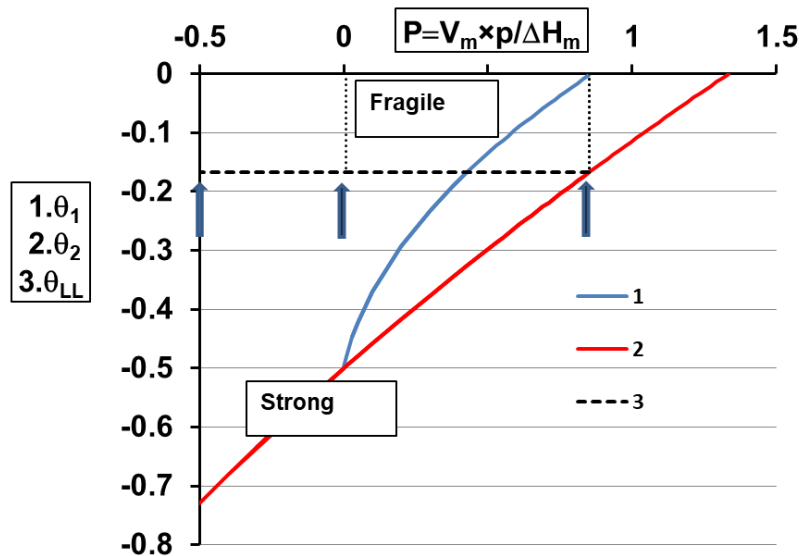


Figure 10 : Phase diagram of supercooled water at pressure p . Curves numbered from 1 to 3: 1- Homogeneous nucleation temperature of strong Phase 1 versus the enthalpy coefficient P induced by the pressure p ; 2- Homogeneous nucleation temperature of strong Phase 2 versus the enthalpy coefficient P induced by the pressure p ; 3- LLPT line separating the fragile liquid phase from the strong one at $\theta_{LL} = -0.16715$; first critical point: $P = -0.5$, $p \approx 175$ MPa; second point: $P = 0.006$, $p \approx 18.3$ MPa; third point at the end of first-order line, $P = 0.8505$, $p \approx 0.31$ GPa.

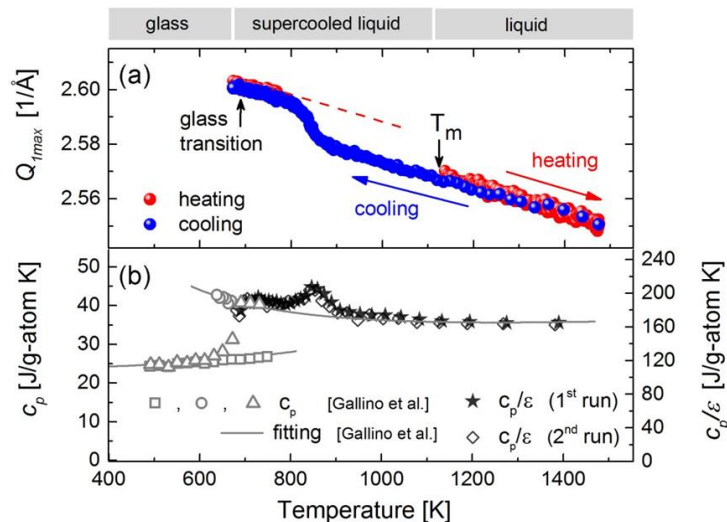


Figure 11: $Zr_{58.5}Cu_{15.6}Ni_{12.8}Al_{10.3}Nb_{2.8}$. Reprinted from [65] with APS permission. (a) Position of the first maximum of $S^*(Q)$, Q_{1max} , during heating of an initially glassy sample and subsequent cooling down to the glassy state. (b) Ratio of specific heat capacity to total hemispherical emissivity c_p/ϵ calculated from

the temperature profile measured in ESL during cooling to the glassy state in comparison with the measured calorimetric cp data of Gallino et al. [66]".

Conclusions:

The thermodynamic parameters of two water phases (Phase 1 and Phase 2), separated by an enthalpy difference depending on $\theta^2=(T-T_m)^2/T_m^2$, have been determined only knowing the formation temperature of a strong glass in Phase 3 where $T_g=136.6$ K, the first-order LLPT was at -45.6°C in confined water under pressure, the compressibility minimum was $+45.6$ °C, the ice melting heat was $\Delta H_m=6000$ J.mole⁻¹, and the melting temperature was 273.1 K.

The LDA phase of strong glass contains an enthalpy excess below $T_g=136.6\text{K}$, resulting from quenching. Consequently (below $T_g=136.6\text{K}$) a sharp, exothermic latent heat is observed through relaxation heating after total decompression at 77K and it can be predicted to occur at temperatures (T_{sg}) in agreement with experimental results. The maximum relaxed enthalpy cannot be higher than its value at the Kauzmann temperature even if the frozen enthalpy is equal to $-0.3704\times\Delta H_m$ at $\theta=-2/3$ without entropy constraint. The enthalpy excess present in the bulk glass at the transformation temperature, leads to partially-amorphous ice instead of fully-relaxed ultrastable glass because the LDA density is too close to that of ice. LDA exists under various forms because any ice having a fusion entropy smaller than 22 J.K.⁻¹mole⁻¹ is crystallized at a temperature equal or larger than its own Kauzmann temperature.

A sharp volume increase from HDA to LDA has been measured at 115.5 K. This transformation temperature corresponds to the Kauzmann temperature $T_K=T_{sg}\cong 115.5$ K. This is the first observation of the Kauzmann temperature of a glass.

Supercooled water is a fragile liquid above a liquid-to-liquid phase transition (LLPT) at $T_{LL}=0.833\times T_m$ and it is transformed into a strong liquid below T_{LL} . The first-order character of LLPT disappears for three pressures equal to approximately -175MPa, 18.3MPa, and 310 MPa. Glass Phase 3 disappears for $p=-175\text{MPa}$ because there is no more glass transition below this negative pressure. For the first time, it has been shown that glass Phase 3 is transformed into a new liquid phase above T_g and that the two liquids separated below T_{LL} are liquid Phase 1 and liquid Phase 3 for -0.175 GPa $<p<+0.31$ GPa. Along the LLPT line, the first-order transition could be exothermic by heating from -175MPa to 18.3MPa and endothermic from 18.3 MPa to 310 MPa.

Double glass transitions are expected under pressure at T_{sg} and T_g when the glass enthalpy is still enhanced by an enthalpy excess. The glass transition occurs at $T_g=0.5\times T_m$ at low pressure ($p<0.31$ GPa) and at $0.632\times T_m$ for HDA under high pressure ($0.31<p<0.6$ GPa). The first-order LDA-HDA phase transitions at T_{sg} under pressure can be predicted, leading to constant volume and enthalpy changes. The predictions correspond to the formation of a new glass Phase 3 with an enthalpy increase equal to the maximum frozen enthalpy ($0.3704\times\Delta H_m$) available at $T=91\text{K}$ ($\theta=-2/3$). This enthalpy change is no longer limited by its value at the Kauzmann temperature because this glass phase is induced by a first-order transition; it has an entropy maximum reduction at T_{sg} which is equal to the available entropy below its own glass transition. The entropy and enthalpy changes at T_{sg} are expected to be recovered in the "no man's land" at this new T_g .

Phase 3 does not disappear but continues to exist as an “ordered” liquid phase above T_g . Ordered liquid Phase 3 is superheated above T_m and disappears at the liquid homogeneous nucleation temperature T_{n+} . This transition is accompanied by a sharp volume decrease under pressure. VHDA is identified as being formed due to the melting of this ordered liquid Phase 3.

All these theoretical findings, using classical nucleation theory completed by an enthalpy difference between two liquids, are fully compatible with the experimental results (without introducing any complementary parameter to ensure the fit). The existence of an ordered liquid above T_g and T_m has been suggested by other authors can now be confirmed, without knowing the nature of its microscopic order at the atomic scale. Ordered phases have to exist in all glass-forming melts giving rise to various glass phases. This work was based on the prediction of homogeneous nucleation temperatures T_{n-} of various liquid and glass phases and it is suggested that they are the formation temperatures of new ordered phases of superclusters followed, after subsequent cooling, by the percolation threshold of dynamical fractal structures above T_g . All these new “ordered phases” still have superheating temperatures T_{n+} at the second homogeneous nucleation temperature T_{n+} above T_m .

Acknowledgments: The author thanks M.I. Ojovan for discussions about the thermodynamic origin of the glass transition. Several tentatives to find the temperature T_{n+} of bulk water using DSC measurements by Gael Moiroux and J.L. Garden in the Neel Institute have failed. Measurements of the temperature gradient along a vertical axis in a recipient filled with water have been made by J. Blanchart. Criticisms of successive anonymous reviewers of Chemical Physics Letters and Chemical Physics have contributed to clarify the presentation of this work.

References

- [1]. R.F. Tournier, *Chem. Phys. Lett.* **665** (2016), 64.
- [2]- K.L. Kearns, K.R. Whitaker, M.D. Ediger, H. Huth, and C. Schick, *J. Chem. Phys.* **133** (2010), 014702.
- [3]- S. Singh, M.D. Ediger, and J.J. de Pablo, *Nature Materials.* **12** (2013), 139.
- [4]- K. Ishii, and H. Nakayama, *Phys. Chem. Chem. Phys.* **16** (2014), 12073.
- [5]- R.F. Tournier, *Chem. Phys. Lett.* **641** (2015), 9.
- [6]- O. Mishima, L.D. Calvert, & E. Whalley, *Nature.* **340** (1984), 393.
- [7]- O. Mishima, L.D. Calvert & E. Whalley, *Nature*, **314** (1985), 76.
- [8]- O. Mishima, *J. Chem. Phys.* **100** (1994), 5910
- [9]- O. Mishima, *Nature.* **384** (1996), 546.
- [10]- O. Mishima, Y. Suzuki, *Nature*, 419 (2002), 599.
- [11]- T. Loerting, W. Schestereider, K. Winkel, C.G. Salzmann, I. Kohl, and E. Mayer, *Phys. Rev. Lett.* **96** (2006), 025702.

- [12]- T. Loerting, and N. Giovambattista, *J. Phys.: Condens. Matter*, **18** (2006), R919.
- [13]- T. Loerting, V.V. Brazhkin, T. Morishita, *Adv. Chem. Phys.* **143** (2009), 29.
- [14]- O.Mishima, *Proc. Jpn. Acad., Ser. B* **86** (2010), 165.
- [15]- W. Kauzmann, *Chem. Rev.* **43** (1948), 219.
- [16]- C.A. Angell, M. Oguni, and W.J. Sichina, *J. Phys. Chem.* **86** (1982), 998.
- [17]- J.A. McMillan and S.C.Los, *Nature*. **206** (1965), 806.
- [18]- M. Sugisaki, H. Suga, and S. Seki, *Bull. Chem. Soc. Jap.* **41** (1968), 2586.
- [19]- C.A. Angell, *Chem. Rev.* **102** (2002), 2627.
- [20]- K. Winkel, E. Mayer, and T. Loerting, *J. Phys. Chem. B*, 115 (2011), 14141.
- [21]- M. Oguni, S. Maruyama, K. Wakabayashi, and A. Nagoe, *Chem. Asian J.* **2** (2007), 514.
- [22]- S. Maruyama, K. Wakabayashi, and M. Oguni, *AIP Conf. Proc.* **708** (2004), 675.
- [23]- P.H. Poole, F. Sciortino, U. Essmann & H.E. Stanley, *Nature*. **360** (1992), 324.
- [24]- D. Liu, Y. Zhang, C.-C. Chen, C.-Y. Mou, P.H. Poole, and S.-H. Chen, *PNAS*. **104** (2007), 9570.
- [25]- V. Holten, C.E. Bertrand, M.A. Anisimov, and J.V. Sengers, *J. Phys. Chem.* **136** (2012), 094507.
- [26]- C.A. Angell, J. Shuppert, and J.C. Tucker, *J. Phys. Chem.* **77** (1971), 3092.
- [27]- S.V. Buldyrev, M. Canpolat, S. Havlin, O. Mishima, M.R. Sadr-Lahijany, A. Scala, F.W. Starr and H. Stanley, *AIP Conf. Proc.* **469** (1999), 243.
- [28]- K. Ito, C.T. Moynihan & C.A. Angell, *Nature*. 398 (1999), 492.
- [29]- V. Holten & M.A. Anisimov, *Sci. Rep.* 2 (2012), 713.
- [30]- J.C. Palmer, F. Martelli, Y. Liu, R. Car, A.Z. Panagiotopoulos, P.G. Benedetti, *Nature*. **510** (2014), 385.
- [31]- Z.R. Sun, G. Sun, Y.X. Chen & L.M. Xu, *Sci. China-Phys. Mech. Astron.* 57 (2014), 810.
- [32]- P.F. McMillan, *J. Mater. Chem.* **14** (2004), 1506.
- [33]- J. Souletie, *J. Phys. France*, **51** (1990), 883.
- [34]- M.I. Ojovan, *J. Exp. Theor. Phys. Lett.* **79** (2004), 632.
- [35]- M.I. Ojovan, *J. Exp. Theor. Phys.* 103 (2006), 819.
- [36]- R.P. Wool, *J. Polymer. Sci B.* 2008, Vol. 46 (2008), 2765.

- [37]- M.I. Ojovan, W. E. Lee, *J. Non-Cryst. Sol.* **356** (2010), 2534.
- [38]- M.I. Ojovan, *J. Non-Cryst. Sol.* **382** (2013), 79.
- [39]- D.S. Sanditov, M.I. Ojovan, *Physica B*, **523** (2017), 96.
- [40]- J.F. Stanzione III, K.E. Strawhecker, R.P. Wool, *J. Non-Cryst. Sol.* **357** (2011), 311.
- [41]- S. Albert, Th. Bauer, M. Michl, G. Biroli, J.-P. Bouchaud, A. Loidl, P. Luckenheimer, R. Tourbot, C. Wiertel-Gasquet, F. Ladieu, *Science*, **352** (2016), 1308.
- [42]- D. Ma, A.D. Stoica, X.-L. Wang, *Nature Mater.* **8** (2016), 30.
- [43]- R.F. Tournier, *Physica B*. **454** (2014), 253.
- [44]- R.F. Tournier, *Phys. B. Condens. Matter.* **392** (2007), 79.
- [45]- R.F. Tournier, J. Bossy, *Chem. Phys. Lett.* **658** (2016), 282.
- [46]- R.F. Tournier, *Chem. Phys. Lett.* **651** (2016) 198; *Chem. Phys. Lett.* **675** (2017), 174.
- [47]- D. Turnbull, *J. Chem. Phys.* **20** (1952), 411.
- [48]- K. Lu, Y. Li, *Phys. Rev. Lett.* **80** (1998), 4474.
- [49]- J.J. Shephard and C.G. Salzmann, *J. Phys. Chem. Lett.* **7** (2016), 2281.
- [50]- R.F. Tournier, *Sci. Technol. Adv. Mater.* **10** (2009), 014501.
- [51]- R.F. Tournier, *Materials*. **4** (2011), 869.
- [52]- R.F. Tournier, *Rev. de Metall.* **109** (2012), 27.
- [53]- R.J. Speedy and C.A. Angell, *J. Chem. Phys.* **65** (1976), 851.
- [54]- R.A. Millero, F.J. Fine, *J. Chem. Phys.* **59** (1973), 5529.
- [55]- C.A. Angell, W.J. Sichina, M. Oguni, *J. Phys. Chem.* **86** (1982), 998.
- [56]- D. Bertolini, M. Cassettari, and G. Salvetti, *Chem. Phys. Lett.* **199** (1985), 553.
- [57]- E. Tombari, C. Ferrari, G. Salvelli, *Chem. Phys. Lett.* **300** (1999), 749.
- [58]- L-M. Wang, S. Borick, C.A. Angell, *J. Non-Cryst. Sol.* **353** (2007), 3829.
- [59]- L. Hornboll, Y. Yue, *J. Non-Cryst. Sol.* **354** (2008), 1862.
- [60]- I.K. Ishii, H. Nakayama, S. Hirabayashi, M. Nakayama, *Chem. Phys. Lett.* **459** (2008), 109.
- [61]- C. Lin, X. Yong, J.S. Tse, J.S. Smith, S.V. Sinogeikin, C. Kenney-Benson, and G. Shen, *Phys. Rev. Lett.* **119** (2017), 135701.

- [62]- J.J. Shephard, S. Ling, G.S. Sosso, A. Michaelides, B. Slater, and C. Salzmann, *J. Chem. Phys. Lett.* **8** (2017), 1645.
- [63]- C. Way, P. Wadhwa, and R. Busch, *Acta Mater.* **55** (2007), 1977.
- [64]- S. Wei, F. Yang, J. Bednarcik, I. Kaban, O. Shuleshova, A. Meyer, & R. Busch, *Nature Comm.* **4** (2013), 2083.
- [65]- M. Stolpe, I. Jonas, S. Wei, Z. Evenson, W. Hembree, F. Yang, A. Meyer, and R. Busch, *Phys. Rev. B* **93** (2016), 014201.
- [66]- I. Gallino, M.B. Shah, and R. Busch, *Acta Mater.* **55** (2007), 1367.
- [67]- D.E. Hare, C.M. Sorensen, *J. Chem. Phys.* **87** (1987), 4840.
- [68]- T. Sorani, J. Arabas, H. Kubota, M. Kijima, *High Temp. High Press.* **32** (2000), 433.
- [69]- O. Mishima, *J. Chem. Phys.* **133** (2010), 144503.
- [70]- C.A. Angell, *Nature Mater.* **13** (2014), 673.
- [71]- M.E.M. Azouzi, C. Ramboz, J.-F. Lenain, and F. Caupin, *Nature Phys.* **9** (2013), 38.